Spin-orbit torque assisted magnetization reversal of 100-nm-long vertical pillar

Syuta Honda[1,2] and Yoshiaki Sonobe[3,4]

[1] Department of Pure and Applied Physics, Kansai University, 3-3-35 Yamate-cho, Suita 564-8680, Japan
[2] Center for Spintronics Research Network, Graduate School of Engineering Science, Osaka University, 1-3 Machikaneyama-cho, Toyonaka 560-8531, Japan
[3] Research Organization for Nano & Life Innovation, Waseda University, Tokyo 162-0041, Japan
[4] Institute of Materials and Systems for Sustainability, Nagoya University, Furo-cho, Chikusa-ku, Nagoya 464-8603, Japan

E-mail: shonda@kansai-u.ac.jp

Abstract (up to 300 words)

Long vertical pillars, with a width of the order of nanometers and with perpendicular shape anisotropy (PSA), have high thermal stability. The advantage of using longer pillars is that they can increase the memory areal density while maintaining robust thermal stability. The current-induced magnetization reversal of long pillars is a significant challenge in spintronic applications such as high-density magnetic memories. However, the magnetization of pillars that are more than 100 nm long has never been reversed by spin-orbit torque (SOT) or spin injection from another ferromagnet. Against this background, we propose a novel magnetization reversal method for pillars based on both SOT and spin transfer torque without using a ferromagnet for spin injection. Furthermore, this SOT-assisted method significantly reduces the reversal time, as was demonstrated by micromagnetic simulation. Using a spin-polarized current and SOT, the magnetization was reversed in pillars with length ≥100 nm. The magnetization of pillars with PSA and those with both high perpendicular magnetic anisotropy and PSA was successfully reversed. The findings of this study are physically novel and significant for practical applications. Consequently, the proposed new writing scheme paves the way for next-generation spintronic devices.

Keywords: spin-orbit torque, PSA-MRAM, magnetization reversal, micromagnetic simulation

1. Introduction

High-speed magnetization reversal of ferromagnetic (FM) materials is a technique that has garnered attention in magnetic memory and other applications featuring FM materials. In particular, the discovery of a current-induced magnetization reversal method for a FM long pillar with a length of several tens of nanometers is expected. This is because the magnetization of long pillars results in high thermal stability [1-4]. The magnetization reversal of pillars is used in perpendicular shape anisotropy magnetic random-access memory (PSA-MRAM) [5-8].

Current-induced magnetization reversal of the thin layer occurs by injecting spin into the layer. One approach is spin injection from another ferromagnet, which is a pin layer (PL) [9-11]. When the current flows through a magnetic tunnel junction (MTJ), comprising a PL/nonmagnetic insulator layer and a FM free layer (FL), the spin is injected into the FL from the PL, and the magnetization of the FL reverses [9-11].

For another approach, there is a spin injection via the spin Hall effect of a heavy metal (HM) when current passes through the HM [12-14]. The injected spin induces a torque to the magnetization of the FL, known as spin-orbit torque (SOT). The SOT can reverse the magnetization of the thin film of which thicknesses are less than 20 nm [15-20]. However, the magnetization reversal for the 100-nm-long pillar with SOT has not been observed.

Recently, the magnetization reversal of a pillar due to spin injection from the PL has been demonstrated using micromagnetic simulation [21]. However, the spin torque acts only on the magnetic moments near the surface of the ferromagnet in which the spin is injected. Hence, there is a maximum size of the FL in which magnetization reversal occurs by spin injection [22]. In other words, the current-induced switching method for a long pillar is not known.

In this study, we propose a novel current-induced reversal method for a PSA-pillar. In this method, we used both SOT and torque of the spin-polarized current flowing through the pillar (spin transfer torque (STT)). This

reverses the magnetization of the pillar without spin injection from the ferromagnet. Hence, the MTJ for magnetization reversal was not necessary. This new flavor method may have high speed, high thermal stability, and high-density magnetic memory.

2. Model and Method

We used a micromagnetic simulation based on the Landau–Lifshitz–Gilbert (LLG) equation to demonstrate the magnetization reversal of a PSA-pillar. We assumed the structure shown in Fig. 1. A pillar was placed on a wire of HM. The magnetic moments of the pillar were subject to the SOT resulting from the spin current polarized in the $+y$-direction, which was injected into the bottom surface of the pillar from the HM. In addition, spin-polarized current flowed through the pillar. The diameter of the pillar D was set to 20 nm, and the length was L ($30\ \text{nm} \le L \le 130\ \text{nm}$). The pillar was subdivided into 1.0-nm-cubic cells. The magnetization in each cell was calculated using the version of the transposed LLG equation shown below (including the SOT and STT terms, which are the third and fourth terms on the right-hand side, respectively) [23-26]:

$$\frac{d\boldsymbol{m}}{dt} = -|\gamma|\,\boldsymbol{m}\times\boldsymbol{B}_{\text{eff}} - \alpha|\gamma|\,\boldsymbol{m}\times(\boldsymbol{m}\times\boldsymbol{B}_{\text{eff}}) - \boldsymbol{m}\times(\boldsymbol{m}\times(-\nabla\cdot\boldsymbol{j}_{\text{sot}})) - \boldsymbol{m}\times(\boldsymbol{m}\times(-\nabla\cdot\boldsymbol{j}_{\text{stt}})). \quad (1)$$

Here, $\boldsymbol{m}$ denotes a unit vector denoting the magnetization direction within each cell, t is the simulation time, γ *is* the gyromagnetic ratio $\gamma = -1.76 \times 10^{11}$ rad s^{-1} T^{-1}, α is the Gilbert damping constant, and $\boldsymbol{B}_{\text{eff}}$ is the effective magnetic field (composed of long-range magnetic dipole–dipole interactions and short-range exchange interactions among the neighboring computational cells).

A simulation code was developed in which the 4th Runge–Kutta method was used for time integration. The parameter values based on the properties of the permalloy were selected as follows: α was set to 0.05, the saturation magnetization M_s was 850 kA m^{-1}, and the exchange stiffness constant A between the adjacent magnetic moments was 13.0 pJ m^{-1} [22,27,28]. These were used to calculate the components of each magnetic field.

$\nabla\cdot\boldsymbol{j}_{\text{sot}}$ is the divergence of the spin current for SOT, defined as $\nabla\cdot\boldsymbol{j}_{\text{sot}} \equiv (0, \partial u/\partial z, 0,)$ and $u \equiv u_0 \exp(-z/\lambda_{\text{FM}})$ [22]. Here, u_0 is the magnitude of the injection velocity of the spin current, polarized in the $+y$-direction, λ_{FM} is the spin-diffusion length of the permalloy, and z is the distance from the bottom of the pillar. The spin diffusion length λ_{FM} was set to 2 nm [29].

$\nabla\cdot\boldsymbol{j}_{\text{stt}}$ is the divergence of the spin current for STT, defined as $\nabla\cdot\boldsymbol{j}_{\text{stt}} \equiv \partial u_z\boldsymbol{m}/\partial z$ [25]. Here, u_z is a component of the spin current velocity $\boldsymbol{u} = (0, 0, u_z) = P\boldsymbol{j}g\mu_B / (2eM_s)$, where $\boldsymbol{j} = (0, 0, j_z)$ is the current density of the spin-polarized current flowing through the pillar, μ_B is the Bohr magneton, and P is the spin polarizability of the spin-polarized current. Eq. (1) is equivalent to a non-adiabatic term of the spin torque considering $\beta = \alpha$ [25,26].

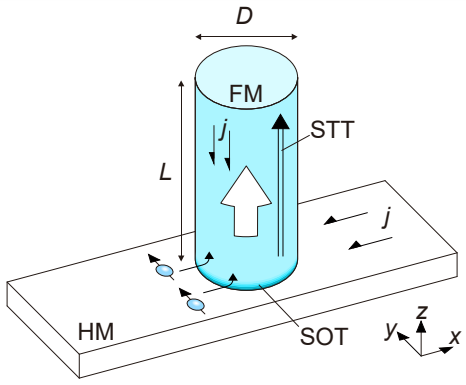

Figure 1. (Color online) Schematic of the simulation structure for magnetization reversal of the FM on the HM owing to SOT and STT.

3. Simulation Results

First, we applied only the SOT of $u_0 = 100$ m s^{-1} to the 60-nm-long pillar ($L = 60$ nm) without the STT. The magnetization was maintained in the initial −z-direction (Fig. 2). After the SOT began to act on the pillar, the magnetic moments in the lower part of the pillar canted (Fig. 2(b,c)). However, the cant of the magnetic moments occurred only in the lower part of the pillar, and the magnetization did not reverse even at $t = 100$ ns (Fig. 2(d)).

When only the STT of $u_z = 100$ m s^{-1} was applied to the 60-nm-long pillar, without the SOT, the magnetization reversed to the +z-direction from the initial −z-direction (Fig. 3). The magnetization reversal time was approximately 12 ns. Here, we defined the time at which the z-component of the averaged unit vector of the magnetic moment at the cells of the top surface of the pillar became 0.9, as the magnetization reversal time t_r. The $|\partial\boldsymbol{m}/\partial z|$ of the magnetic moments is not just zero near the bottom of the pillar. Hence, the STT acted on the magnetic moments, and the magnetization reversed slowly. Figure 3(e) shows the time-dependence of the magnetization of the pillar when the STT continued to be applied after magnetization reversal. Here, $\langle m_z \rangle$ is the z-component of the averaged unit vector of magnetic moment. After the first magnetization reversal, the magnetization returned to the −z-direction. This magnetization reversal process is similar

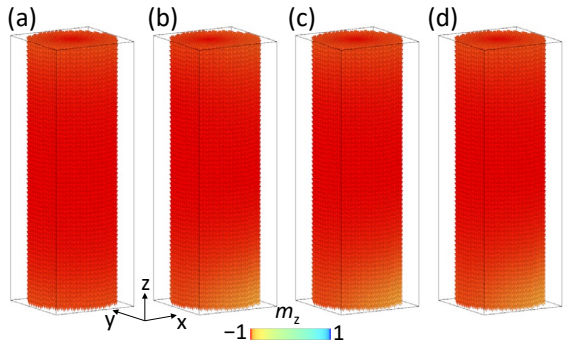

Figure 2. (Color online) Snapshots of the magnetization in the 60-nm-long pillar with the SOT of u_0 = 100 m s^{-1} without the STT at t = (a) 0, (b) 1, (c) 2, and (d) 100 ns. The z-component of each magnetic moment in the pillar was plotted with a colored small arrow.

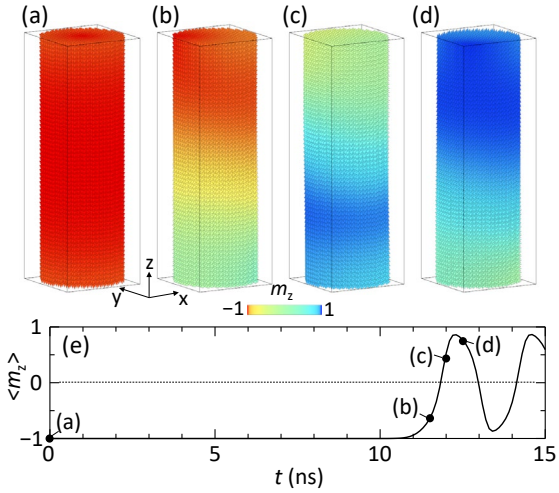

Figure 3. (Color online) Snapshots of the magnetization reversal process in the 60-nm-long pillar with the STT of u_z = 100 m s^{-1} without the SOT at t = (a) 0, (b) 11.5, (c) 12.0, and (d) 12.5 ns. The z-component of each magnetic moment in the pillar was plotted with a colored small arrow. (e) Time-dependence of the z-component of the averaged unit vector of magnetic moment <m_z>.

to the process of the domain wall injection into the nanowire with STT [30,31]

Next, we applied both the SOT of u_0 = 100 m s^{-1} and STT of u_z = 100 m s^{-1} to the 60-nm-long pillar. Figure 4 shows snapshots of the magnetization reversal process. Before the SOT and STT were applied to the pillar, the magnetization pointed in the −z-direction (Fig. 4(a)). The SOT and STT began to act on the magnetization simultaneously (t = 0). Subsequently, the magnetization at the lower part of the pillar first began rotating by the SOT (Fig. 4(b)). Because the pillar is long, the domain is generated in the lower part. The magnetic moments turn in the +z-direction because of the dipole–dipole interactions near the bottom of the pillar while the domain moved to the upper side of the pillar owing to the STT (Fig. 4(c)). Consequently, the magnetization reversed in the +z-direction from the −z-direction because of the SOT and STT (Fig. 4(d)).

Figure 4(e) shows the time dependence of the magnetization of the 60-nm-long pillar when the SOT and STT continue to be applied after magnetization reversal. The magnetization reversed at $t_r \approx 1.8$ ns. This magnetization reversal time is much smaller than $t_r \approx 12$ ns when only the STT is applied. Because the spin-polarized direction of the spin current for the SOT was perpendicular to the initial magnetized direction of the pillar, the SOT acted strongly on the magnetization at the bottom of the pillar [10,32] and rotated on the magnetization. Thus, the SOT increases $|\partial \boldsymbol{m}/\partial z|$ at the bottom. The STT propagated the canting magnetization with assistance from the SOT. Consequently, the magnetization was quickly reversed.

After the first magnetization reversal, the magnetization returned to the −z-direction at $t \approx 2.7$ ns. The magnetization continued to reverse thereafter. When the SOT and STT stopped, the magnetization reversal also stopped. The four broken curves in Fig. 4(e) indicate the time dependence of the magnetization when the SOT and STT stopped at t = 1.2, 1.6, 2.0, and 2.4 ns. The magnetization approached the +z-direction or −z-direction after the SOT and STT stopped.

Figure 4(f) shows the time-dependence of the magnetic energy. The energy is plotted as the energy difference between the magnetization of t and t = 0 ($\Delta E = E(t) - E(0)$). When <m_z> approached 1 and −1, ΔE decreased. Meanwhile, when <m_z> approached 0, ΔE increased. Hence, the magnetization approached the +z-direction or −z-direction after the SOT and STT stopped. This is similar to the previous study for the magnetization reversal of the thin film [33].

With both SOT and STT acting on the pillar, whether the magnetization reverses depended on the length of the pillar L. Figure 5(a) shows the magnetization reversal time t_r of the pillar with $40 \le L \le 130$ nm with SOT of u_0 = 100 m s^{-1} and STT of u_z = 100 m s^{-1}. The direction of magnetization is maintained in the initial direction of the pillar that is less than 54 nm, as shown by the gray region in Fig. 5(a). In these cases, a domain was not generated in the lower part of the pillar. Therefore, the magnetization was maintained in the initial direction. When the pillar had a length of $54 < L < 114$ nm, the magnetization was reversed. The magnetization reversal time t_r tended to increase as the pillar length L increased. However, this difference was

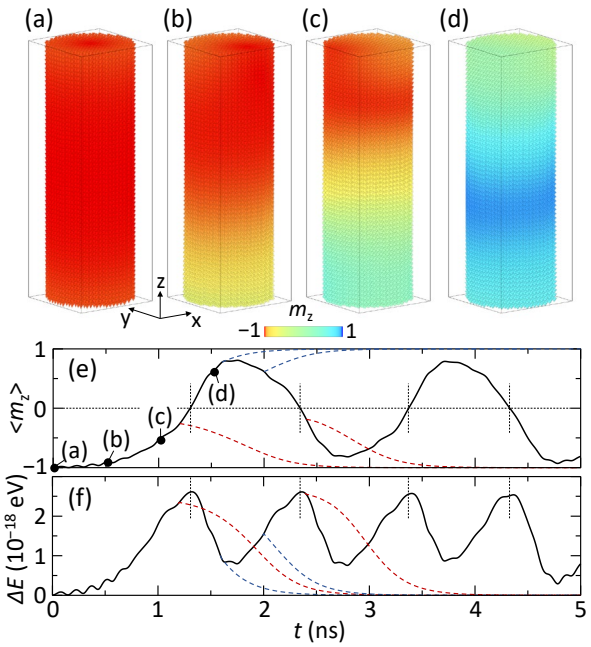

Figure 4. (Color online) Snapshots of the magnetization reversal process in the 60-nm-long pillar with both SOT of u_0 = 100 m s^{-1} and STT of u_z = 100 m s^{-1} at t = (a) 0, (b) 0.5, (c) 1.0, and (d) 1.5 ns. The z-component of each magnetic moment in the pillar was plotted with a colored small arrow. Time-dependence of the z-component of (e) the averaged unit vector of magnetic moment $\langle m_z \rangle$ and (f) the energy difference ($\Delta E = E(t) - E(0)$). The four broken curves in (e) and (f) indicate $\langle m_z \rangle$ and ΔE after the SOT and STT stopped at t = 1.2, 1.6, 2.0, and 2.4 ns, respectively.

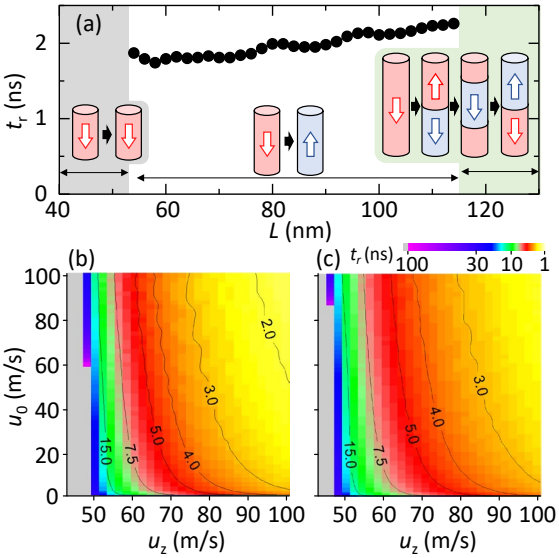

Figure 5. (Color online) Magnetization reversal time t_r for the pillars of (a) 40 nm ≤ L ≤ 130 nm with SOT of u_0 = 100 m s^{-1} and STT of u_z = 100 m s^{-1}, and L = (b) 60 and (c) 100 nm as a function of u_0 and u_z. In the pillar with L < 54 nm, which is shown by the grey region in (a), the magnetization direction was maintained in the initial direction. The gray regions in (b) and (c) indicate that the magnetization was not reversed even at 100 ns.

small, and the magnetization was reversed in approximately 2 ns. When the pillar had a length of 116 nm ≤ L, two domains were produced. The two domains maintained even 5 nm after the SOT and STT stopped.

Figures 5(b, c) show the dependence of the magnetization reversal times t_r for the 60- and 100-nm-length pillars on SOT and STT, respectively. The reversal time increased with decreasing STT and SOT values. The magnetization was reversed in the pillar with an STT of u_z larger than 50 m/s. By applying the SOT, the reversal time rapidly decayed. Consequently, the SOT-assisted method can significantly reduce the reversal time.

We introduce one for the reasons of the magnetization reversal. Figure 6(a) shows the magnetic moments in the cross section of the yz-surface including the center axis of the 100-nm-length pillar with SOT of u_0 = 100 m s^{-1} and STT of u_z = 100 m s^{-1} at t = 0.89 ns. At this time, the magnetic moments near the bottom pointed in the approximately +y-direction owing to the influence of the SOT. Because the magnetic moments at the edge of the pillar pointed to the outside of the pillar, the magnetic moments at one edge slightly have the +z-components (Fig. 6(b)). These moments with +z-components propagate to the upper side owing to the influence of the STT (Fig. 6(c, d)). Subsequently, the area with the magnetic moments of the +z-direction was extended by the STT, and the magnetization was subsequently reversed.

From the examples in which the magnetization reverse in the pillar with the short length (L < 54 nm), we show the magnetic moments of the 40-nm-length pillar with SOT of u_0 = 100 m s^{-1} and STT of u_z = 100 m s^{-1} at t = 1.0 ns, as in Fig. 6(e)). Additionally, we show the z-component of the magnetic moments (m_z) along the center line of the pillar when m_z of the bottom was closest to 0 in the 25-, 40-, and 100-nm-length pillars, of which the values of time are t = 0.88, 1.0, and 0.15 ns, respectively. In the cases of the 25- and 40-nm-length pillars, the magnetic moments were maintained m_z < 0. As the wire length became shorter, the position of $m_z \sim -1$ approached the bottom of the wire (Fig. 6(f)). These suggest that a larger SOT is required to rotate the magnetic moment at the bottom of the pillar to m_z = 0 in the shorter pillar.

Finally, we show the diameter-dependence of the magnetization reversal times. Figure 7 shows the

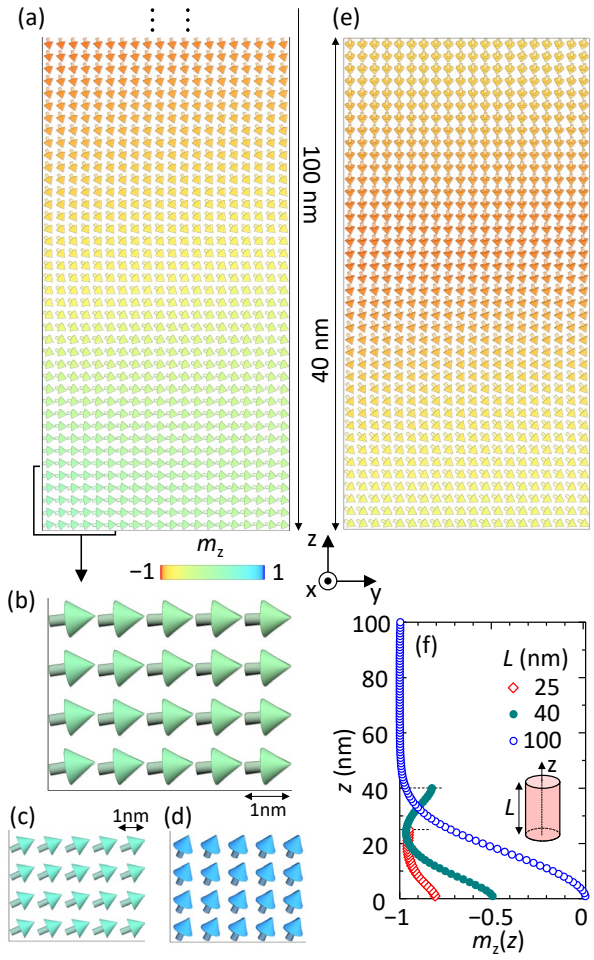

Figure 6. (Color online) Magnetic moments of the 100- and 40-nm-length pillars with SOT of u_0 = 100 m s^{-1} and STT of u_z = 100 m s^{-1}. (a) Magnetic moments of 40 nm on the underside of the 100-nm-length pillar at t = 0.88 ns. Magnetic moment of bottom edge of the 100-nm-length pillar at (b) t = 0.88, (c) 1.10, and (d) 1.15 ns. (e) Magnetic moments of the 40-nm-length pillar at t = 1.0 ns. (f) z-component of magnetic moments along the center line ($m_z(z)$) of the 100-, 40-, and 25-nm-length pillars at t = 0.88, 1.0, and 0.15 ns, respectively, here z denotes the distance from the bottom of the pillar. The small arrows in (a–e) indicate the direction of the magnetic moments.

magnetization reversal times t_r of pillar D = 15, 20, and 25 nm with SOT of u_0 = 100 m s^{-1} and STT of u_z = 100 m s^{-1}. When the magnetization reversed, the diameter-dependence of the magnetization reversal time was small. The smaller the diameter, the smaller the minimum and maximum lengths of the pillar where the magnetization reversal occurs.

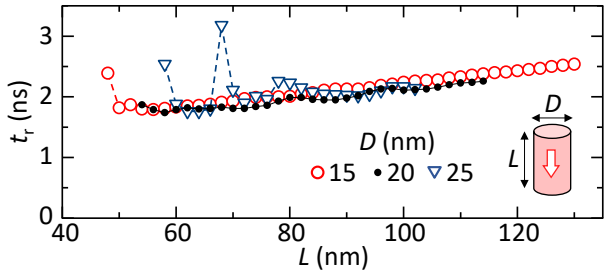

Figure 7. (Color online) Magnetization reversal time t_r of the pillar with diameter (D) of 15, 20, and 25 nm. t_r for the 20-nm-diameter, which are small closed circles, are the same graphs shown in Fig. 5(a).

4. Discussion

We demonstrated magnetization reversal of the PSA-pillar. We discuss with a focus on applications using the pillar, namely PSA-MRAM. In PSA-STT-MRAM, strong spin injection from the PL is required to reverse the magnetization of the pillar [21]. Our magnetization reversal method does not require spin injection from another ferromagnet. An element of MRAM can comprise our proposed writing structure and another reading structure.

Various structures, such as MTJ, GMR, and Hall sensors, can be used as the reading structure. We assumed MTJ, which is practically used in MRAM. When the MTJ is used for reading, a perpendicularly magnetized layer, such as a CoFeB layer [34-36], may be used as the PL of the MTJ. However, an MTJ composed of the pillar, which has a perpendicular anisotropy K_u = 0, shown in Fig. 8(a), may have an MR ratio smaller than that of an MTJ of CoFeB/MgO/CoFeB. An MTJ composed of a thin layer with perpendicular anisotropy or interfacial perpendicular magnetic anisotropy (IPMA) on the pillar of K_u = 0 [37-39], as shown in Fig. 8(b), may have an MR ratio larger than that of an MTJ with K_u = 0. This structure also has higher thermal stability. We simulated the magnetization reversal for a 60-nm-long pillar in which the upper part has a high K_u of 1.0 MJ m^{-3} or 3.0 MJ m^{-3}, and the other part has K_u of 0. (High K_u materials have K_u of the order of 1.0 MJ m^{-3} [40-43].) Figure 8(c) shows the reversal time t_r for a pillar with a high K_u, with both SOT of u_0 = 100 m s^{-1} and the STT of u_z = 100 m s^{-1} applied. The magnetization reversed in the pillar with $d \leq$ 53 (20) nm for K_u = 1.0 (3.0) MJ m^{-3}. Here, d denotes the length of the region with a high K_u. These reversal times were approximately equal to or slightly smaller than 1.79 ns of the reversal time for the 0-K_u 60-nm-long pillar (d = 0). This result may be similar to

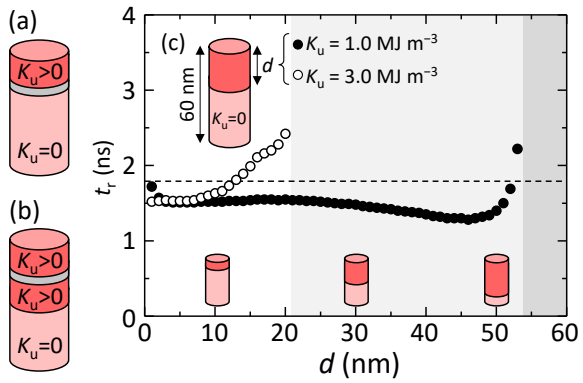

Figure 8. (Color online) Schematics of (a) MTJ composed of the pillar of $K_u = 0$, and (b) pillar including $K_u > 0$. (c) Simulation results of the magnetization reversal time t_r for the 60-nm-long hybrid pillar with the diameter of 20 nm in which the region d from the upper surface has the perpendicular anisotropy of $K_u = 1.0$ and 3.0 MJ m^{-3}, with both SOT of $u_0 = 100$ m s^{-1} and STT of $u_z = 100$ m s^{-1}. In the pillar with $K_u = 3.0$ (1.0) MJ m^{-3} with d in the right (dark) gray regions, the magnetized direction was maintained. A dotted line of $t_r = 1.79$ ns denotes the magnetization reversal time of the 60-nm-long 0-K_u pillar ($d = 0$).

the magnetization reversal for an exchange coupled composite (ECC) media and an exchange spring effect [44,45] in which a high K_u layer is used for robust thermal stability and a high TMR ratio; and a soft layer of $K_u \sim 0$ can significantly reduce the magnetization reversal time. Moreover, optimization of the exchange coupling strength between the two layers may improve the reversal time.

The magnetization did not reverse in the 60-nm-long pillar with both PSA and PMA (d = 60 nm). The magnetization in such a pillar reverses owing to the spin injection from the PL [21].

Two domains were produced in a long pillar, such as the 20-nm-diameter-pillar with 116 nm $\leq L$, being acted on by the SOT and STT. This is a negative result of magnetization reversal for the PSA-MRAM. However, this will be used for multi-bit MRAM [46,47] or vertical racetrack memory [48,49].

5. Conclusion

In conclusion, the magnetization of pillars can be reversed by the torque of the spin injection from the HM (SOT) and the torque of the spin-polarized current flowing through the pillar (STT). This magnetization reversal does not use spin injection from another ferromagnet. This was demonstrated using the micromagnetic approach. The magnetization was reversed in the pillars with a length of ≥100 nm, such as 20-nm-diameter-pillar with approximately 50 nm < L < 116 nm. Magnetization reversal occurred in both the pillar with PSA and the pillar with high K_u and PSA. When the pillar was longer than approximately 116 nm, a magnetic domain was produced. These results could be applied to device designs of magnetic memories, such as PSA-MRAM and multi-bit MRAM. This SOT-assisted method significantly reduces the reversal time. In addition, the new flavor method with the ECC structure may maintain high speed, high thermal stability, and high-density magnetic memory. The magnetized direction can be controlled by the timing of the application of the two torques. It is expected that the magnetization reversal of the pillar with the method described in this paper will be observed experimentally in the future.

Acknowledgments

This work was supported by the Japan Society for the Promotion of Science KAKENHI (Grant Number 20H02607), the Kansai University Fund for Supporting Outlay Research Centers 2020, and CREST, Japan Science and Technology Agency (Grant Number JPMJCR21C1).

References

[1] K. Watanabe, B. Jinnai, S. Fukami, H. Sato, and H. Ohno, *Nat. Commun.*, **9**, 663 (2018). https://doi.org/10.1038/s41467-018-03003-7

[2] B. Jinnai, J. Igarashi, K. Watanabe, T. Funatsu, H. Sato, S. Fukami, H. Ohno, *IEDM 2020*, 20432448, San Francisco, USA (2020). https://doi.org/10.1109/IEDM13553.2020.9371972

[3] Y. Lu, R. A. Altman, A. Marley, S. A. Rishton, P. L. Trouilloud, Gang Xiao, W. J. Gallagher, and S. S. P. Parkin, *Appl. Phys. Lett.*, **70**, 2610 (1997). https://doi.org/10.1063/1.118933

[4] N. Perrissin, S. Lequeux, N. Strelkov, A. Chavent, L. Vila, L. D. Buda-Prejbeanu, S. Auffret, R. C. Sousa, I. L. Prejbeanu, and B. Dieny, *Nanoscale*, **10**, 12187 (2018). https://doi.org/10.1039/C8NR01365A

[5] P. Wiśniowski, J. M. Almeida, S. Cardoso, N. P. Barradas, and P. P. Freitas, *J. Appl. Phys.*, **103**, 07A910 (2008). https://doi.org/10.1063/1.2838626

[6] N. Perrissin, G. Gregoire, S. Lequeux, L. Tillie, N. Strelkov, S. Auffret, L. D. Buda-Prejbeanu, R. C. Sousa, L. Vila, B. Dieny, and I. L. Prejbeanu, *J. Phys. D: Appl. Phys.*, **52**, 234001 (2019). https://doi.org/10.1088/1361-6463/ab0de4

[7] N. Perrissin, N. Cacoilo, G. Gregoire, S. Lequeux, L. Tillie, N. Strelkov, A. Chavent, S. Auffret, L. D. Buda-Prejbeanu, R. C. Sousa, L. Vila, I. L. Prejbeanu, and B. Dieny, *J. Phys. D: Appl.*

Phys., **52**, 505005 (2019). https://doi.org/10.1088/1361-6463/ab4215

[8] S. Lequeux, N. Perrissin, G. Grégoire, L. Tillie, A. Chavent, N. Strelkov, L. Vila, L. D. Buda-Prejbeanu, S. Auffret, R. C. Sousa, I. L. Prejbeanu, E. D. Russo, E. Gautier, A. P. Conlan, D. Cooper, and B. Dieny, *Nanoscale*, **12**, 6378 (2020). https://doi.org/10.1039/C9NR10366J

[9] K. L. Wang, J. G. Alzate, and P. K. Amiri, *J. Phys. D: Appl. Phys.*, **46**, 074003 (2013). https://doi.org/10.1088/0022-3727/46/7/074003

[10] J. C. Slonczewski, *J. Magn. Magn. Mater.*, **159**, L1 (1996). https://doi.org/10.1016/0304-8853(96)00062-5

[11] L. Berger, *Phys. Rev. B*, **54**, 9353 (1996). https://doi.org/10.1103/PhysRevB.54.9353

[12] M. M. Decker, M. S. Wörnle, A. Meisinger, M. Vogel, H. S. Körner, G. Y. Shi, C. Song, M. Kronseder, and C. H. Back, *Phys. Rev. Lett.*, **118**, 257201 (2017). https://doi.org/10.1103/PhysRevLett.118.257201

[13] K. Ando, S. Takahashi, K. Harii, K. Sasage, J. Ieda, S. Maekawa, and E. Saitoh, *Phys. Rev. Lett.*, **101**, 036601 (2008). https://doi.org/10.1103/PhysRevLett.101.036601

[14] A. V. Khvalkovskiy, V. Cros, D. Apalkov, V. Nikitin, M. Krounbi, K. A. Zvezdin, A. Anane, J. Grollier, and A. Fert, *Phys. Rev. B*, **87**, 020402(R) (2013). https://doi.org/10.1103/PhysRevB.87.020402

[15] S. Fukami, T. Anekawa, C. Zhang and H. Ohno, *Nature Nanotech.*, **11**, 621 (2016). https://doi.org/10.1038/nnano.2016.29

[16] J. Han, A. Richardella, S. A. Siddiqui, J. Finley, N. Samarth, and L. Liu, *Phys. Rev. Lett.*, **119**, 077702 (2017). https://doi.org/10.1103/PhysRevLett.119.077702

[17] C. K. Safeer, E. Jué, A. Lopez, L. B.-Prejbeanu, S. Auffret, S. Pizzini, O. Boulle, I. M. Miron, and G. Gaudin, *Nature Nanotech.*, **11**, 143 (2016). https://doi.org/10.1038/nnano.2015.252

[18] Y.-C. Lau, D. Betto, K. Rode, J. M. D. Coey, and P. Stamenov, *Nature Nanotech.*, **11**, 758 (2016). https://doi.org/10.1038/nnano.2016.84

[19] Luqiao Liu, O. J. Lee, T. J. Gudmundsen, D. C. Ralph, and R. A. Buhrman, *Phys. Rev. Lett.*, **109**, 096602 (2012). https://doi.org/10.1103/PhysRevLett.109.096602

[20] E. Grimaldi, V. Krizakova, G. Sala, F. Yasin, S. Couet, G. S. Kar, K. Garello, and P. Gambardella, *Nature Nanotech.*, **15**, 111 (2020). https://doi.org/10.1038/s41565-019-0607-7

[21] N. Caçoilo, S. Lequeux, B. M. S. Teixeira, B. Dieny, R. C. Sousa, N. A. Sobolev, O. Fruchart, I. L. Prejbeanu, and L. D. Buda-Prejbeanu, *Phys. Rev. Appl*., **16**, 024020 (2021). https://doi.org/10.1103/PhysRevApplied.16.024020

[22] S. Honda and H. Itoh, *J. Nanoscience and Nanotechnology*, **12**, 8662 (2012). https://doi.org/10.1166/jnn.2012.6481

[23] Y. Nakatani, Y. Uesaka, and N. Hayashi, *Jpn. J. Appl. Phys.*, **28**, 2485 (1989). https://doi.org/10.1143/JJAP.28.2485

[24] S. Zhang and Z. Li, *Phys. Rev. Lett.*, **93**, 127204 (2004). https://doi.org/10.1103/PhysRevLett.93.127204

[25] A. Thiaville, Y. Nakatani, J. Miltat, and Y. Suzuki, *Europhys. Lett.*, **69**, 990 (2005). https://doi.org/10.1209/epl/i2004-10452-6

[26] S. E. Barnes and S. Maekawa, *Phys. Rev. Lett.*, **95**, 107204 (2005). https://doi.org/10.1103/PhysRevLett.95.107204

[27] M. Buess, T. Haug, M. R. Scheinfein, and C. H. Back, *Phys. Rev. Lett.*, **94**, 127205 (2005). https://doi.org/10.1103/PhysRevLett.94.127205

[28] D. X. Niu, X. Zou, J. Wu, and Y. B. Xu, *Appl. Phys. Lett.*, **94**, 072501 (2009). https://doi.org/10.1063/1.3076108

[29] S. Dubois, L. Piraux, J. M. George, K. Ounadjela, J. L. Duvail, and A. Fert, *Phys. Rev. B*, **60**, 477 (1999). https://doi.org/10.1103/PhysRevB.60.477

[30] D. R. Rodrigues, N. Sommer, and K. E.-Sitte, *Phys. Rev. B*, **101**, 224410 (2020). https://doi.org/10.1103/PhysRevB.101.224410

[31] A. K. Jana and S. N. Jammalanadaka, *Nanotecnology*, **33**, 105707 (2021). https://doi.org/10.1088/1361-6528/ac23f4

[32] S. Honda, H. Itoh, *J. Magn. Soc. Jpn.*, **37**, 338 (2013) (in Japanese) https://doi.org/10.3379/msjmag.1308R001

[33] F. Wang, X. Zhang, Z. Zhang, and Y. Liu, J. Magn. Magn. Mat., **527**, 167757 (2021). https://doi.org/10.1016/j.jmmm.2021.167757

[34] K. Tsunekawa, D. D. Djayaprawira, M. Nagai, H. Maehara, S. Yamagata, N. Watanabe, S. Yuasa, Y. Suzuki, K. Ando, *Appl. Phys. Lett*. **87**, 072503 (2005). https://doi.org/10.1063/1.2012525

[35] S. Ikeda, J. Hayakawa, Y. Ashizawa, Y. M. Lee, K. Miura, H. Hasegawa, M. Tsunoda, F. Matsukura, and H. Ohno, *Appl. Phys. Lett*., **93**, 082508 (2008). https://doi.org/10.1063/1.2976435

[36] D. C. Worledge, G. Hu, D. W. Abraham, J. Z. Sun, P. L. Trouilloud, J. Nowak, S. Brown, M. C. Gaidis, E. J. O'Sullivan, and R. P. Robertazzi, *Appl. Phys. Lett.*, **98**, 022501 (2011). https://doi.org/10.1063/1.3536482

[37] J. F. Sierra, V. V. Pryadun, F. G. Aliev, S. E. Russek, M. G.-Hernández, E. Snoeck, and V. V. Metlushk, *Appl. Phys. Lett*., **93**, 172510 (2008). https://doi.org/10.1063/1.3005644

[38] S. Ikeda, K. Miura, H. Yamamoto, K. Mizunuma, H. D. Gan, M. Endo, S. Kanai, J. Hayakawa, F. Matsukura, and H. Ohno, *Nature Materials*, **9**, 721 (2010). https://doi.org/10.1038/nmat2804

[39] B. Dieny and M. Chshiev, *Rev. Mod. Phys.*, **89**, 025008 (2017). https://doi.org/10.1103/RevModPhys.89.025008

[40] S. Fukami, T. Suzuki, Y. Nakatani, N. Ishiwata, M. Yamanouchi. Ikeda, N. Kasai, and H. Ohno, *Appl. Phys. Lett.*, **98**, 082504 (2011). https://doi.org/10.1063/1.3558917

[41] M. Yamanouchi, A. Jander, P. Dhagat, S. Ikeda, F. Matsukura, H. Ohno, *IEEE Magn. Lett.,* **2**, 3000304 (2011). https://doi.org/10.1109/LMAG.2011.2159484

[42] Y. Yamada, W. P. Van Drent, E. N. Abarra, and T. Suzuki, *J. Appl. Phys*., 83, 6527 (1998). https://doi.org/10.1063/1.367917

[43] S. Mizukami, F. Wu, A. Sakuma, J. Walowski, D. Watanabe, T. Kubota, X. Zhang, H. Naganuma, M. Oogane, Y. Ando, and T. Miyazaki, *Phys. Rev. Lett.*, **106**, 117201 (2011). https://doi.org/10.1103/PhysRevLett.106.117201

[44] J.-P. Wang, W. Shen, and J. Bai, *IEEE trans. magn.*, **41**, 3181 (2005) https://doi.org/10.1109/TMAG.2005.855278

[45] V. R. Reddy, O. Crisan, A. Gupta, A. Banerjee, and V. Kuncser, *thin solid films*, **520**, 2184 (2012). https://doi.org/10.1016/j.tsf.2011.10.143

[46] W. Kang, W. Zhao, Z. Wang, Y. Zhang, J.-O. Klein, C. Chappert, Y. Zhang, and D. Ravelosona, *IEEE Trans. Magn*., **50**, 3400207 (2014) https://doi.org/10.1109/TMAG.2014.2300836

[47] Y. M. Hung, T. Li, R. Hisatomi, Y. Shiota, T. Moriyama, and T. Ono, *J. Magn. Soc. Jpn.*, **45**, 6 (2021). https://doi.org/10.3379/msjmag.2011R002

[48] S. S. P. Parkin, M. Hayashi, and L. Thoms, *Science*, **320**, 190 (2008). https://doi.org/10.1126/science.1145799

[49] S. Honda, Y. Sonobe, and S. J. Greaves, *J. Phys. D: Appl. Phys.*, **54**, 135002 (2021). https://doi.org/10.1088/1361-6463/abd060